Available online at www.sciencedirect.com
ScienceDirect
Journal of Sound and Vibration 303 (2007) 371–390
JOURNAL OF SOUND AND VIBRATION
www.elsevier.com/locate/jsvi

Transient dynamic analysis of a floating beam–water interaction system excited by the impact of a landing beam

J.Z. Jin, J.T. Xing*

Ship Science, School of Engineering Sciences, University of Southampton, Highfield, Southampton SO17 1BJ, UK

Received 22 February 2006; received in revised form 17 January 2007; accepted 23 January 2007
Available online 26 March 2007

Abstract

An aircraft, idealised as an elastic beam with supporting system, lands with speed on an aircraft carrier or floating airport. The floating platform is idealised as a flexible beam floating in an infinite water domain. The water is assumed incompressible and inviscid. The surface disturbance satisfies a linear free surface wave condition and an undisturbed condition at infinity. A mathematical model is developed to describe this complex fluid–structure interactive dynamical system, which exhibits strong coupling between the system's components. An effective numerical scheme is established assuming that the two beam-like structures are two solid substructures with motions represented by their respective mode functions and the infinite fluid domain is modelled by a boundary element scheme. A mixed mode function-boundary element method is developed to solve the transient dynamics of the system in terms of the time histories of the beam displacement responses and water pressure. The presented data demonstrates the applicability of the developed mathematical model and numerical approach and some insights of the complex interactive process exhibited by the system.

1. Introduction

Approximately, 70% of the Earth's surface is covered by ocean. The utilisation of ocean space for development is of great importance to future advancement. For example, the concept of a floating airport or runway in coastal waters using a very large floating structure has become attractive during recent years to ease congestion on land. The typical dimensions of such a platform could be several kilometres long and only a few metres deep. For such a sheet-like structure, its bending rigidity will be relatively small so that its elastic deflection becomes a crucial parameter in assessing feasibility and the development of a safe design.

When designing a floating airport, the naval architect needs to address not only the structure's response to ocean waves but also its transient dynamic response due to the impulsive and moving load excited by the landing and take-off of an aircraft. The development of the mathematical model and the time domain solution of the complex, interactive dynamical problem necessitates inter-disciplinary studies relating to the aircraft, floating airport, fluid and their interactions.

*Corresponding author. Tel.: +44 23 8059 6549; fax: +44 23 8059 3299.
E-mail address: j.t.xing@ship.soton.ac.uk (J.T. Xing).

0022-460X/$ - see front matter © 2007 Elsevier Ltd. All rights reserved.
doi:10.1016/j.jsv.2007.01.026

Only a limited number of studies on this kind of problem have been reported to date. For example, using a NASTRAN programme, Watanabe and Utsunomiya [1] presented the numerical results of the elastic responses of a very large circular floating structure excited by impulsive loading. Transient responses of an infinite long elastic runway excited by a moving load were investigated by Kim and Webster [2] and Yeung and Kim [3]. The former studied the added drag caused by the flexibility of the runway whereas the latter focused on the resonance phenomenon caused by the accumulation of energy near the moving load. Ohmatsu [4] presented a calculation method based on Fourier transforms, adopting the frequency-domain response function to analyse the responses of an elastic floating structure influenced by an arbitrary changing load. Endo and Yago [5] proposed an alternative method using Fourier transforms, in which the time dependent memory-effect function describing hydrodynamic forces was evaluated from frequency-domain results. Subsequently the differential equations describing the elastic motions of the floating structure were solved directly in the time domain by means of a finite element method. Kashiwagi [6] simulated the transient responses of a floating airport during landing and take-off of a Boeing 747-400 jumbo jet. The time-domain mode-expansion method used by Kashiwagi [7] was adopted and special attention was paid to study the added drag during take-off.

However, in all of these studies it was assumed that a prescribed external load is applied to the floating airport to represent the dynamic process of landing or take-off of an aircraft but no interactions between the aircraft and the floating airport are considered. Following the preliminary investigations and numerical results presented by Xing and Jin [8,9], in which the landing of a mass–spring–damper system on a floating rigid body and a floating elastic beam was considered, respectively, this paper develops and investigates the mathematical model of an integrated aircraft–floating structure–fluid interaction system and the numerical scheme to solve its complex dynamic behaviour. To reduce complexity of analysis, the aircraft and floating airport are idealised as two elastic beams and a two-dimensional (2-D) infinite fluid domain is assumed. The proposed approach, with suitable modifications, can be extended to tackle a fully three-dimensional (3-D) problem modelling the interaction of a flexible structure landing on a floating structure.

2. Governing equations

Fig. 1 schematically illustrates an elastic beam of length L, thickness h and draught d floating on the calm water surface of a 2-D infinite water domain. It is assumed that an aircraft, idealised by an elastic beam and a vertical supporting system fixed at its centre, lands and travels on a floating platform, idealised by the floating flexible beam. The supporting system consists of a linear spring of stiffness K, original length l_K and a damper of damping coefficient C. The 2-D Cartesian coordinate system $O-XZ$ as shown is fixed in space at point O, which coincides with the mass centre of the floating beam initially. The $O-X$ axis is horizontal and $O-Z$ axis is vertically upward. The coordinate system $o-xz$ with its axis $o-x$ parallel to the axis $O-X$ is initially fixed at the mass centre of the landing beam. However, this system is

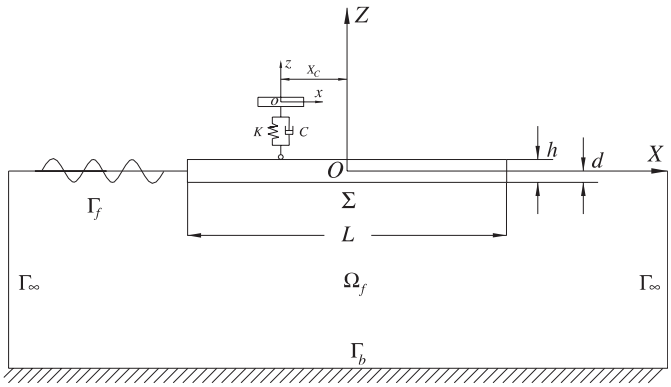

Fig. 1. A landing beam–floating beam–water interaction system impacted by the landing beam.

a moving system with a horizontal velocity equal to the instant horizontal velocity V_X of the mass centre of the landing beam at time t.

The coordinate systems $\bar{O}-\bar{X}\bar{Z}$ and $\bar{o}-\bar{x}\bar{z}$ denote two systems fixed in the floating beam and the landing beam, respectively, such that at initial time $t=0$, they coincide with the two systems $O{-}XZ$ and $o{-}xz$, respectively. Systems $\bar{O}-\bar{X}\bar{Z}$ and $\bar{o}-\bar{x}\bar{z}$ are two Lagrangian frames of reference to describe the motions of the two solid bodies, respectively.

The landing beam lands at point $(\bar{X}_0, \bar{Z}_0)$ on the surface of the floating beam with initial velocities V_{Z0} and V_{X0} in the vertical and horizontal direction at time $t=0$ and then travels to a new position $(\bar{X}_C, \bar{Z}_C)$ at time t. It is assumed that the landing beam is subject to a constant landing resistance F_X in the horizontal direction and therefore it travels with a negative acceleration on the floating beam in the positive direction of $O{-}X$ axis until stopping. Obviously, the horizontal velocity V_X of the mass centre of the landing beam is not constant and the moving coordinate system $o{-}xz$ is a non-inertial system in which the inertial forces of the landing beam are assessed when dealing with the relative deformation of the landing beam in this moving coordinate system.

To simplify this problem, we assume that (1) there is no separation between the lower end of the supporting system and the floating beam during the landing process, (2) the supporting system has sufficient large horizontal stiffness to remain vertical, (3) there is no initial deformation of the landing beam relative to the moving coordinate system $o{-}xz$, (4) the dynamic displacements of the landing and floating beams are negligibly small compared to the translation displacement of the mass centre of the landing beam. Therefore, the contact point between the lower end of the supporting system and the floating beam can be calculated using only the horizontal equation of motion of the mass centre of the landing beam.

The governing equations describing the dynamics of this landing beam–floating beam–water interaction system are as follows.

2.1. Fluid domain

As shown in Fig. 1, a 2-D domain Ω_f is occupied by the water of mass density ρ, which is assumed incompressible and inviscid with its motion irrotational. $\Gamma_b, \Gamma_\infty, \Gamma_f$ and Σ denote the sea bed, a suitable far field, the free surface and the wetted interaction boundaries of the water domain Ω_f, respectively. The velocity potential $\phi(X, Z, t)$ of the fluid satisfies the following equations defined under the fixed coordinate system $O{-}XZ$.

Laplace's equation:

$$\nabla^2\phi = 0 \quad \text{in } \Omega_f. \tag{1}$$

Linearized pressure–velocity potential relation:

$$\bar{p} = -\rho\partial\phi/\partial t - \rho g Z, \tag{2}$$

where $\bar{p}$ represents the water pressure and g denotes gravitational acceleration.

Boundary conditions:

$$\partial^2\phi/\partial t^2 + g\partial\phi/\partial Z = 0 \quad \text{on } \Gamma_f, \tag{3}$$

$$\partial\phi/\partial Z = 0 \quad \text{on } \Gamma_b, \tag{4}$$

$$\partial\phi/\partial X = 0 \quad \text{on } \Gamma_\infty. \tag{5}$$

2.2. Landing beam

The motion of the landing beam is governed by the following two equations: one describes its small elastic/rigid motions relative to the moving coordinate system $o{-}xz$ and the other describes the large horizontal motion of its mass centre in the fixed coordinate system $O{-}XZ$.

The equation of motion governing the dynamics of the landing beam relative to the moving system $o-xz$ is represented as

$$E_l I_l \partial^4 w/\partial \bar{x}^4 + m_l \partial^2 w/\partial t^2 = -F_i \delta(\bar{x} - \bar{x}_C) - m_l g, \tag{6}$$

where

$$\delta(\bar{x} - \bar{x}_C) = \begin{cases} 0, & \bar{x} \neq \bar{x}_C, \\ \infty, & \bar{x} = \bar{x}_C. \end{cases} \tag{7}$$

Here $\delta()$ is the Dirac delta function. Also, $E_l I_l$, m_l denote the bending stiffness, mass per unit length of the landing beam, respectively. $w(\bar{x}, t)$ represents the vertical deflection of the landing beam in the $o-xz$ coordinate system, $\bar{x}_C$ defines the coordinate of the mass centre of the landing beam and F_i describes the interaction force between the two beams which will be discussed later.

The boundary conditions applicable at the free ends of the landing beam are

$$\partial^2 w/\partial \bar{x}^2 = 0, \quad \partial^3 w/\partial \bar{x}^3 = 0, \tag{8}$$

which confirm the vanishing of bending moment and shearing force at the free ends of the beam.

The equation of the horizontal translation of the mass centre of the landing beam relative to the fixed coordinate system $O-XZ$ is represented as

$$F_X = (m_l l) a_X, \quad V_X = a_X t + V_{X0}, \quad \bar{X}_C = a_X t^2/2 + V_{X0} t + \bar{X}_0, \tag{9}$$

where l is the length of the landing beam and a_X describes the horizontal acceleration of the mass centre of the landing beam relative to the system $O-XZ$.

2.3. Floating beam

The motion of the floating beam relative to the fixed coordinate system $O-XZ$ is governed by the dynamic equation:

$$E_f I_f \partial^4 W/\partial \bar{X}^4 + m_f \partial^2 W/\partial t^2 = \tilde{p} + F_i \delta\big(\bar{X} - \bar{X}_C\big) - m_f g. \tag{10}$$

Here, $E_f I_f$, m_f represent the bending stiffness and mass per unit length of the floating beam, respectively. $W\big(\bar{X}, t\big)$ denotes the vertical deflection of the floating beam and $\tilde{p}$ describes the traction force on the wet interface of the floating beam. Again, the appropriate boundary conditions at the free ends of the floating beam are

$$\partial^2 W/\partial \bar{X}^2 = 0, \quad \partial^3 W/\partial \bar{X}^3 = 0. \tag{11}$$

The interaction force F_i consists of a spring force and a damping force which can be obtained using the relative displacement and velocity between the two ends of the supporting system. It is given as

$$F_i = K\big[w(\bar{x}_C, t) - W\big(\bar{X}_C, t\big)\big] + C\big[\partial w(\bar{x}_C, t)/\partial t - \partial W\big(\bar{X}_C, t\big)/\partial t\big]. \tag{12}$$

2.4. Fluid–structure interaction interface condition

On the fluid–floating beam interaction interface Σ, the vertical velocities of both water and the floating beam are consistent and the traction force acting on the bottom of floating beam equals the water pressure. Therefore the velocity potential ϕ, the dynamic displacement of the floating beam W, the traction force $\tilde{p}$ on the floating beam and the water pressure $\bar{p}$ satisfy the following conditions:

$$\partial \phi/\partial Z = \partial W/\partial t, \quad \bar{p} = \tilde{p}. \tag{13}$$

2.5. Initial conditions

At time $t = 0$, the fluid and floating beam are assumed to be in their stationary equilibrium position. The mass centre of the landing beam has an initial velocity V_{Z0} and V_{X0} in the fixed coordinate system $O{-}XZ$ but it is assumed that its relative deformation to the moving system $o{-}xz$ is neglected. These initial conditions are expressed as follows:

Fluid:

$$\phi = 0, \quad \partial\phi/\partial t = 0. \tag{14}$$

Floating beam:

$$W = 0, \quad \partial W/\partial t = 0. \tag{15}$$

Landing beam:

$$w = 0, \quad \partial w/\partial t = V_{Z0}, \quad \dot{Z}_C = V_{Z0}, \quad \dot{X}_C = V_{X0}, \tag{16}$$

where (X_C, Z_C) denotes the coordinates of the mass centre of the landing beam in the fixed system $O{-}XZ$ and an over dot represents a derivative with respect to time t.

3. Mode equations of solid substructures

3.1. Mode functions of a free–free beam

The mode functions of a structure may be obtained by a theoretical, numerical or an experimental approach. In this paper, the theoretical modes [10] for the bending of a uniform beam with free ends are adopted and they are given as

$$f_m(x) = \begin{cases} 1/2, & m = 1, \\ \dfrac{1}{2}\left\{\dfrac{\cosh\left(\mu_m x/a\right)}{\cosh\,\mu_m} + \dfrac{\cos\left(\mu_m x/a\right)}{\cos\,\mu_m}\right\}, & m = 3, 5, \ldots, \end{cases}$$

$$f_m(x) = \begin{cases} \sqrt{3}x/2a, & m = 2, \\ \dfrac{1}{2}\left\{\dfrac{\sinh\left(\mu_m x/a\right)}{\sinh\,\mu_m} + \dfrac{\sin\left(\mu_m x/a\right)}{\sin\,\mu_m}\right\}, & m = 4, 6, \ldots, \end{cases} \tag{17}$$

where a is the half-length of beam and μ_m denote positive real roots of the eigenvalue equation:

$$\begin{cases} \tan\,\mu_m + \tanh\,\mu_m = 0, & m = 3, 5, \ldots, \\ \tan\,\mu_m - \tanh\,\mu_m = 0, & m = 4, 6, \ldots. \end{cases} \tag{18}$$

The orthogonal condition of these mode functions is given by

$$\int_{-a}^{a} f_i(x) f_j(x)\,\mathrm{d}x = \begin{cases} 0, & i \neq j, \\ a/2, & i = j. \end{cases} \tag{19}$$

The natural modes of a free–free beam given in Eq. (17) are known as the dry modes, which are different from the wet modes of the beam–water interaction system as reported by Xing et al. [11]. However, as it is well known that for a linear beam its all normalised natural modes construct a complete and orthogonal space in which any motions of the beam in dry case or wet case can be described. Based on this conclusion and the mode superposition method, the dynamic deflection of the landing and floating beams are expressed in terms of their dry mode functions to transform their dynamic equations into the corresponding mode equations in their mode space, respectively, as follows.

3.2. Mode equation of landing beam

The deflection of landing beam is represented by the form

$$w(\bar{x},t)=\boldsymbol{\psi}(\bar{x})\mathbf{q}(t), \tag{20}$$

where the mode vector is $\boldsymbol{\psi}(\bar{x})=[f_{l1}(\bar{x}),f_{l2}(\bar{x}),\ldots,f_{lM_l}(\bar{x})]$, M_l denotes the number of retained modes whereas $\mathbf{q}(t)=[q_1(t),q_2(t),\ldots,q_{M_l}(t)]^{\mathrm{T}}$ is an unknown time-dependent coordinate vector.

Substituting Eq. (20) into Eq. (6), multiplying both sides of the modified Eq. (6) by $\boldsymbol{\psi}(\bar{x})^{\mathrm{T}}$ and using the orthogonal condition as well as the free boundary conditions of the beam, the mode equation for landing beam is given by

$$\mathbf{M}^{(l)}\ddot{\mathbf{q}}(t)+\mathbf{K}^{(l)}\mathbf{q}(t)=\mathbf{F}_i^{(l)}+\mathbf{F}_g^{(l)}, \tag{21}$$

where

$$\begin{aligned}
\mathbf{M}^{(l)}&=\int_{-l/2}^{l/2}\boldsymbol{\psi}^{\mathrm{T}}m_l\boldsymbol{\psi}\,\mathrm{d}\bar{x}=\frac{m_l l}{4}\mathbf{I}^{(l)},\\
\mathbf{K}^{(l)}&=\int_{-l/2}^{l/2}\left(\boldsymbol{\psi}^{(2)}\right)^{\mathrm{T}}E_lI_l\boldsymbol{\psi}^{(2)}\,\mathrm{d}\bar{x}=\frac{m_l l}{4}\boldsymbol{\Lambda}^{(l)},\\
\mathbf{F}_i^{(l)}&=-\int_{-l/2}^{l/2}\boldsymbol{\psi}^{\mathrm{T}}F_i\delta(\bar{x}-\bar{x}_C)\,\mathrm{d}\bar{x},\\
\mathbf{F}_g^{(l)}&=-\int_{-l/2}^{l/2}\boldsymbol{\psi}^{\mathrm{T}}m_l g\,\mathrm{d}\bar{x}
\end{aligned} \tag{22}$$

and $\mathbf{I}^{(l)}$ represents the unit matrix of order M_l, $\boldsymbol{\Lambda}^{(l)}$ denotes a diagonal matrix of natural frequencies of the landing beam such that

$$\boldsymbol{\Lambda}^{(l)}=\mathrm{diag}\left(\omega_l^2\right). \tag{23}$$

3.3. Mode equation of floating beam

The deflection of the floating beam is expressed as

$$W\left(\bar{X},t\right)=\boldsymbol{\Phi}\left(\bar{X}\right)\mathbf{Q}(t), \tag{24}$$

where the mode vector is $\boldsymbol{\Phi}(\bar{X})=[f_{f1}(\bar{X}),f_{f2}(\bar{X}),\ldots,f_{fM_f}(\bar{X})]$, M_f represents the number of the retained modes and $Q(t)=[Q_1(t),Q_2(t),\ldots,Q_{M_f}(t)]^{\mathrm{T}}$ is the unknown time-dependent coordinate vector.

The application of the mode transformation as same as to derive Eq. (21) for the landing beam gives the mode equation of the floating beam as follows:

$$\mathbf{M}^{(f)}\ddot{\mathbf{Q}}(t)+\mathbf{K}^{(f)}\mathbf{Q}(t)=\mathbf{F}_i^{(f)}+\mathbf{F}_g^{(f)}+\mathbf{F}_d^{(f)}, \tag{25}$$

where

$$\begin{aligned}
\mathbf{M}^{(f)}&=\int_{-L/2}^{L/2}\boldsymbol{\Phi}^{\mathrm{T}}m_f\boldsymbol{\Phi}\,\mathrm{d}\bar{X}=\frac{m_f L}{4}\mathbf{I}^{(f)},\\
\mathbf{K}^{(f)}&=\int_{-L/2}^{L/2}\left(\boldsymbol{\Phi}^{(2)}\right)^{\mathrm{T}}E_fI_f\boldsymbol{\Phi}^{(2)}\,\mathrm{d}\bar{X}=\frac{m_f L}{4}\boldsymbol{\Lambda}^{(f)},\\
\mathbf{F}_i^{(f)}&=\int_{-L/2}^{L/2}\boldsymbol{\Phi}^{\mathrm{T}}F_i\delta\left(\bar{X}-\bar{X}_C\right)\mathrm{d}\bar{X},
\end{aligned}$$

$$\mathbf{F}_g^{(f)} = -\int_{-L/2}^{L/2} \mathbf{\Phi}^{\mathrm{T}} m_f g \, \mathrm{d}\bar{X},$$
$$\mathbf{F}_d^{(f)} = \int_{-L/2}^{L/2} \mathbf{\Phi}^{\mathrm{T}} \tilde{p} \, \mathrm{d}\bar{X} \tag{26}$$

and $\mathbf{I}^{(f)}$ is the unit matrix of order M_f and $\mathbf{\Lambda}^{(f)}$ is a diagonal matrix of natural frequencies of the floating beam such that

$$\mathbf{\Lambda}^{(f)} = \mathrm{diag}\left(\omega_f^2\right). \tag{27}$$

On substituting Eqs. (20) and (24) into Eq. (12), the interaction force F_i between the two beams becomes

$$F_i = K\left[\boldsymbol{\psi}(\bar{x}_C)\mathbf{q}(t) - \mathbf{\Phi}\left(\bar{X}_C\right)\mathbf{Q}(t)\right] + C\left[\boldsymbol{\psi}(\bar{x}_C)\dot{\mathbf{q}}(t) - \mathbf{\Phi}\left(\bar{X}_C\right)\dot{\mathbf{Q}}(t)\right]. \tag{28}$$

Eqs. (21) and (25) can be merged to form the coupled equation in the following matrix form:

$$\begin{bmatrix} \mathbf{M}^{(l)} & \mathbf{0} \\ \mathbf{0} & \mathbf{M}^{(f)} \end{bmatrix} \begin{bmatrix} \ddot{\mathbf{q}} \\ \ddot{\mathbf{Q}} \end{bmatrix} + \begin{bmatrix} \mathbf{C}^{(ll)} & \mathbf{C}^{(lf)}(t) \\ \mathbf{C}^{(fl)}(t) & \mathbf{C}^{(ff)}(t) \end{bmatrix} \begin{bmatrix} \dot{\mathbf{q}} \\ \dot{\mathbf{Q}} \end{bmatrix} + \begin{bmatrix} \mathbf{K}^{(l)} + \mathbf{K}^{(ll)} & \mathbf{K}^{(lf)}(t) \\ \mathbf{K}^{(fl)}(t) & \mathbf{K}^{(f)} + \mathbf{K}^{(ff)}(t) \end{bmatrix} \begin{bmatrix} \mathbf{q} \\ \mathbf{Q} \end{bmatrix} = \begin{bmatrix} \mathbf{F}_g^{(l)} \\ \mathbf{F}_g^{(f)} + \mathbf{F}_d^{(f)} \end{bmatrix}, \tag{29}$$

where

$$\begin{aligned}
\mathbf{K}^{(ll)} &= \boldsymbol{\psi}^{\mathrm{T}}(\bar{x}_C) K \boldsymbol{\psi}(\bar{x}_C), \\
\mathbf{K}^{(lf)}(t) &= -\boldsymbol{\psi}^{\mathrm{T}}(\bar{x}_C) K \mathbf{\Phi}\left(\bar{X}_C\right), \\
\mathbf{K}^{(fl)}(t) &= -\mathbf{\Phi}^{\mathrm{T}}\left(\bar{X}_C\right) K \boldsymbol{\psi}(\bar{x}_C), \\
\mathbf{K}^{(ff)}(t) &= \mathbf{\Phi}^{\mathrm{T}}\left(\bar{X}_C\right) K \mathbf{\Phi}\left(\bar{X}_C\right), \\
\mathbf{C}^{(ll)} &= \boldsymbol{\psi}^{\mathrm{T}}(\bar{x}_C) C \boldsymbol{\psi}(\bar{x}_C), \\
\mathbf{C}^{(lf)}(t) &= -\boldsymbol{\psi}^{\mathrm{T}}(\bar{x}_C) C \mathbf{\Phi}\left(\bar{X}_C\right), \\
\mathbf{C}^{(fl)}(t) &= -\mathbf{\Phi}^{\mathrm{T}}\left(\bar{X}_C\right) C \boldsymbol{\psi}(\bar{x}_C), \\
\mathbf{C}^{(ff)}(t) &= \mathbf{\Phi}^{\mathrm{T}}\left(\bar{X}_C\right) C \mathbf{\Phi}\left(\bar{X}_C\right).
\end{aligned} \tag{30}$$

4. Boundary element equation of the fluid domain

The fundamental solution or Green function $G(p, q)$ of the 2-D infinite fluid domain is defined by the following equation [12]:

$$\begin{aligned}
&\nabla^2 G = 2\pi\delta(p-q) \quad \text{in } \Omega_f, \\
&\frac{\partial G}{\partial n} = 0 \quad \text{on} \quad \infty \quad \text{boundary}.
\end{aligned} \tag{31}$$

Here, ∞ boundary includes the boundaries at infinity of the 2-D infinite fluid domain and n denotes a unit outer normal of the ∞ boundary. In this investigation, infinite deep water is considered, which simplifies the analysis by avoiding boundary element calculations on the sea bed but does not lose the generality of the method because consideration of finite deep water only introduces an extra boundary element idealisation on the sea bed. Therefore, the sea bed boundary Γ_b is also considered at infinity in this analysis. For applications in deriving the boundary element equation later, the involved boundary conditions satisfied by the Green function are highlighted as

$$\frac{\partial G}{\partial X} = 0 \quad \text{on } \Gamma_\infty, \tag{32}$$

$$\frac{\partial G}{\partial Z} = 0 \quad \text{on } \Gamma_b, \tag{33}$$

where p is the field point at coordinate (X_p, Z_p) and q is the source point at coordinate (X_q, Z_q) in the fluid domain.

The Green function $G(p, q)$ is given as [12,13]

$$G(p,q) = \ln r_{pq}, \tag{34}$$

where $r_{pq} = \sqrt{(X_p - X_q)^2 + (Z_p - Z_q)^2}$. This function $G(p, q)$ does not satisfy the free surface condition given in Eq. (3) and the wet interaction interface condition in Eq. (13). However, the function $G(p, q)$ and the potential ϕ of velocity satisfy the conditions required by the Green's third identity [12,14]. The Green function G in Eq. (34) and the potential ϕ of velocity are now substituted into the Green third identity which gives that

$$\phi_p = \frac{1}{2\pi}\int_l \left(\phi_q \frac{\partial \ln r_{pq}}{\partial n_q} - \ln r_{pq}\frac{\partial \phi_q}{\partial n_q}\right) \mathrm{d}l_q, \tag{35}$$

where $l = \Gamma_f + \Gamma_\infty + \Gamma_b + \Sigma$ is the boundary of the fluid domain and n_q is the unit outer normal vector along the boundary, ϕ_p and ϕ_q represent the velocity potentials at the field point p and the source point q, respectively. Eq. (35) is a generalised equation, which holds for any specified boundary conditions of a problem. Now, we consider our problem requiring the defined conditions given in Eqs. (3)–(5), (13), (32) and (33). Substituting these conditions into Eq. (35) and letting the field point p approach the boundary of the fluid domain, we find that

$$\pi\phi_p = \int_{\Gamma_f}\left(\phi_q \frac{\partial \ln r_{pq}}{\partial n_q} + \frac{1}{g}\ln r_{pq}\frac{\partial^2 \phi_q}{\partial t^2}\right)\mathrm{d}l_q + \int_\Sigma \left(\phi_q \frac{\partial \ln r_{pq}}{\partial n_q} - \ln r_{pq}\frac{\partial W_q}{\partial t}\right)\mathrm{d}l_q. \tag{36}$$

In this equation, only free surface and wet interface are involved, which is the result using Eqs. (4), (5), (32) and (33). It should be mentioned that in numerical simulations, a real infinite boundary cannot be realised. We choose an outside boundary of the fluid, which is sufficient far from the floating structure as a numerical 'infinite' boundary. This approximation can be accepted for this transient dynamic analysis in which the interested vibration information appears during a very short time period from the aircraft landing starting. At the end of this short time period, the disturbance of the water cannot reach the chosen numerical 'infinite' boundary.

For simplicity, a constant boundary element is used to model the fluid boundary. It is assumed that the boundaries Γ_f and Σ of the fluid domain are divided into $2N_f$ (each side N_f) and N_Σ constant elements, respectively. We adopt $\bar{N}_f$ and $\bar{N}_\Sigma$ to denote two sets of the identifying numbers of the elements on the free surface Γ_f and fluid–structure interaction interface Σ, respectively. The velocity potential of each element is assumed to have a constant value at its centre. For example, the velocity potential in the jth element is represented by $\phi_j(t)$. Allowing the discretization of Eq. (36), it can be expressed as

$$\pi\phi_i(t) = \sum_{j=1}^{2N_f+N_\Sigma}\phi_j(t)\int_{l_j}\frac{\partial \ln r_{iq}}{\partial n_q}\mathrm{d}l_q + \frac{1}{g}\sum_{j\in\bar{N}_f}\ddot{\phi}_j(t)\int_{l_j}\ln r_{iq}\,\mathrm{d}l_q - \int_\Sigma \dot{W}_q \ln r_{iq}\,\mathrm{d}l_q,$$
$$i = 1, 2, \ldots, 2N_f + N_\Sigma, \tag{37}$$

which can be rewritten in the matrix form

$$\mathbf{G}\ddot{\mathbf{\Psi}} + \mathbf{H}\mathbf{\Psi} = \tilde{\mathbf{G}}\,\dot{\mathbf{Q}}(t). \tag{38}$$

The representative elements, denoted by $()_{ij}$, of the matrices $\mathbf{G}$, $\mathbf{H}$ and $\tilde{\mathbf{G}}$ are, respectively, given as

$$G_{ij} = \begin{cases} \dfrac{1}{g}\int_{l_j} \ln r_{iq}\,\mathrm{d}l_q, & j \in \bar{N}_f, \\ 0 & j \notin \bar{N}_f, \end{cases} \quad i,j = 1,2,\ldots,2N_f + N_\Sigma,$$

$$H_{ij} = \int_{l_j} \frac{\partial \ln r_{iq}}{\partial n_q}\mathrm{d}l_q - \pi\delta_{ij}, \quad i,j = 1,2,\ldots,2N_f + N_\Sigma,$$

$$\tilde{G}_{ij} = \int_{\Sigma} \ln r_{iq} f_{fj}\,\mathrm{d}l_q, \quad i = 1,2,\ldots,2N_f + N_\Sigma, \quad j = 1,2,\ldots,M_f, \tag{39}$$

where

$$\delta_{ij} = \begin{cases} 0, & i \neq j, \\ 1, & i = j. \end{cases} \tag{40}$$

The unknown vector $\mathbf{\Psi}$ is expressed in terms of $\mathbf{\Psi}_1$ on the left free surface, $\mathbf{\Psi}_2$ on the fluid–structure interaction interface and $\mathbf{\Psi}_3$ on the right free surface such that

$$\begin{aligned} \mathbf{\Psi} &= \left[\mathbf{\Psi}_1^{\mathrm{T}}, \mathbf{\Psi}_2^{\mathrm{T}}, \mathbf{\Psi}_3^{\mathrm{T}}\right]^{\mathrm{T}}, \\ \mathbf{\Psi}_1 &= \left[\phi_1(t), \phi_2(t), \ldots, \phi_{N_f}(t)\right]^{\mathrm{T}}, \\ \mathbf{\Psi}_2 &= \left[\phi_{N_f+1}(t), \phi_{N_f+2}(t), \ldots, \phi_{N_f+N_\Sigma}(t)\right]^{\mathrm{T}}, \\ \mathbf{\Psi}_3 &= \left[\phi_{N_f+N_\Sigma+1}(t), \phi_{N_f+N_\Sigma+2}(t), \ldots, \phi_{2N_f+N_\Sigma}(t)\right]^{\mathrm{T}}. \end{aligned} \tag{41}$$

5. Mixed mode function-boundary element equations

From Eqs. (2), (13) and (26), the force vector of water pressure applied to the floating beam is obtained as

$$\mathbf{F}_d^{(f)} = -C^d\ddot{\mathbf{\Psi}}_2 - \mathbf{K}^d\mathbf{Q}(t) + \bar{\mathbf{F}}_d^{(f)}, \tag{42}$$

where a representative element of matrix $\mathbf{C}^d$ is calculated by

$$C_{ij}^d = \rho\int_{l_j} f_{fi}\,\mathrm{d}l, \quad i = 1,2,\ldots,M_f, j \in \bar{N}_\Sigma$$

and matrix $\mathbf{K}^d$ and vector $\bar{\mathbf{F}}_d^{(f)}$ are given as

$$\begin{aligned} \mathbf{K}^d &= \textstyle\int_{-L/2}^{L/2} \mathbf{\Phi}^{\mathrm{T}}\rho g\mathbf{\Phi}\,\mathrm{d}\bar{X}, \\ \bar{\mathbf{F}}_d^{(f)} &= \textstyle\int_{-L/2}^{L/2} \mathbf{\Phi}^{\mathrm{T}}\rho g d\,\mathrm{d}\bar{X}. \end{aligned} \tag{43}$$

On substituting Eq. (42) into Eq. (29), we find that

$$\begin{bmatrix} \mathbf{M}^{(l)} & \mathbf{0} \\ \mathbf{0} & \mathbf{M}^{(f)} \end{bmatrix}\begin{bmatrix} \ddot{\mathbf{q}} \\ \ddot{\mathbf{Q}} \end{bmatrix} + \begin{bmatrix} \mathbf{C}^{(ll)} & \mathbf{C}^{(lf)}(t) \\ \mathbf{C}^{(fl)}(t) & \mathbf{C}^{(ff)}(t) \end{bmatrix}\begin{bmatrix} \dot{\mathbf{q}} \\ \dot{\mathbf{Q}} \end{bmatrix} + \begin{bmatrix} \mathbf{K}^{(l)} + \mathbf{K}^{(ll)} & \mathbf{K}^{(lf)}(t) \\ \mathbf{K}^{(fl)}(t) & \mathbf{K}^{(f)} + \mathbf{K}^{(ff)}(t) + \mathbf{K}^d \end{bmatrix}\begin{bmatrix} \mathbf{q} \\ \mathbf{Q} \end{bmatrix} = \begin{bmatrix} \mathbf{F}_g^{(l)} \\ -\mathbf{C}^d\dot{\mathbf{\Psi}}_2 \end{bmatrix}. \tag{44}$$

Eqs. (38) and (44) provide a set of mixed mode function-boundary element equations to describe the dynamics of this complex interaction system.

6. Numerical solution

Because of the time-dependent stiffness and damping matrices in Eq. (44), the problem studied herein has a strong transient characteristic and a time integration approach has to be adopted. The time integration equations used in the numerical method are derived in Appendix A. Using these equations given in Appendix A and starting from the initial conditions given in Eqs. (14)–(16), we can complete the time integration of the mixed mode function-boundary element equations modelling the airplane–floating structure–water interaction system subject to airplane landing impacts.

Assume that the values of the required variables at time $t-\Delta t$ have been obtained, for example $t-\Delta t = 0$ representing the initial time at which the initial conditions are prescribed, Fig. 2 shows a flow chart to integrate the numerical equations derived in Appendix A to obtain the values of all required variables at time t. Following completing all calculations for time step t, the calculation can go to the next time step for time $t+\Delta t$. This calculation process shown in Fig. 2 continues until reaching the final time interested in the analysis of the problem.

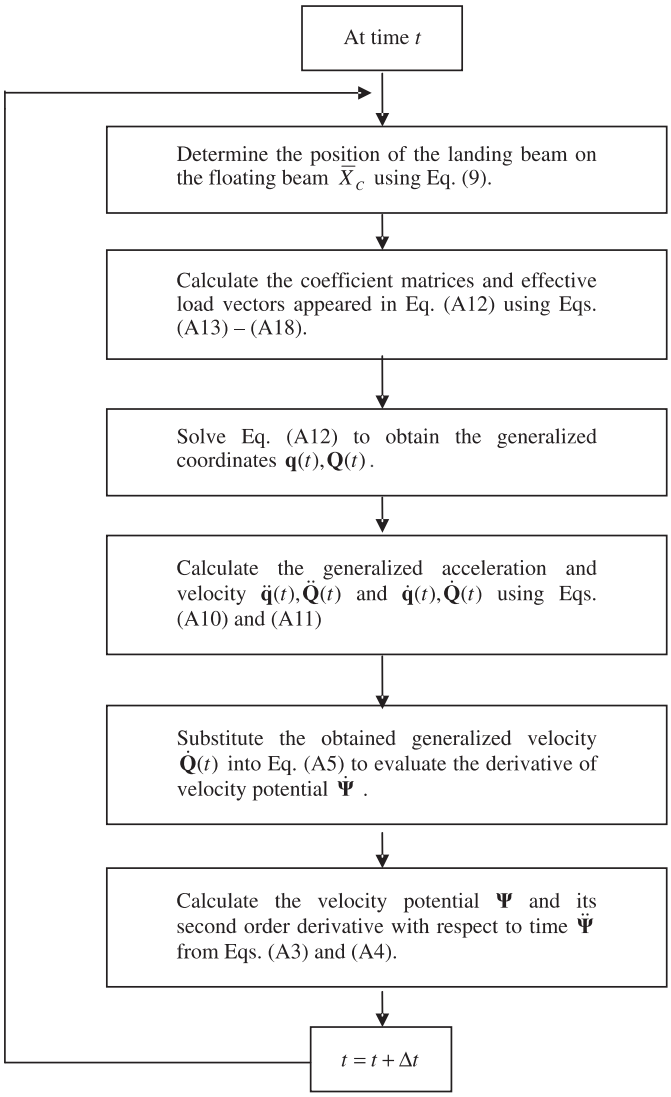

Fig. 2. Flow chart of time integration process.

7. Numerical results

7.1. A simulation for a car running test

To validate the mixed mode function-boundary element method presented herein, a numerical simulation of a car running test conducted by Endo and Yago [5] is implemented.

In Endo and Yago's test, a small carriage of mass 6.91 kg was towed on the rail of a plate model shown in Fig. 3. The plate whose geometrical and physical data are listed in Table 1, floated on the free surface of a towing tank of length 40 m, width 27.5 m and water depth 1.9 m. The rail is shifted 0.18 m from the centreline of the plate. The carriage moved with a constant towing velocity 0.61 m/s along the positive direction of $O-X$ axis. The vertical displacements at five points Z1, Z3, Z5, Z7, Z9 along the centerline of the plate model were measured.

To simulate this test using the developed model of landing beam–floating beam–water interaction system, the landing beam is assumed to have a very large bending stiffness $E_l I_l = 2 \times 10^{10}\,\mathrm{N\,m^2}$, a mass density $m_l = 6.91\,\mathrm{kg/m}$ and length $l = 1\,\mathrm{m}$, which approximately provides a rigid body of total mass 6.91 kg like the carriage used in the test. The supporting system is reduced to an extremely strong spring of $K = 2.0 \times 10^{10}\,\mathrm{N/m}$ and $C = 0\,\mathrm{Ns/m}$. The landing beam has a zero vertical landing velocity but only a constant horizontal velocity $V_{X0} = 0.61\,\mathrm{m/s}$ same as the towing velocity in the experiment. As the very large water depth-plate draught ratio $1.9/0.0163 = 116$ in the experiment, the water depth is assumed to be infinite in the numerical simulation. The fluid surface area in the numerical simulation is a rectangular of length $50 \times 9.75\,\mathrm{m}$, width 1.95 m and its centre at point O.

In the numerical calculation, the involved fluid boundaries are divided into 2040 constant elements of $N_\Sigma = 40$ elements on the wet interface and $2N_f = 2000$ elements on the free surface. The numbers of modes retained for the two elastic beams are both 16. The time increment step $\Delta t = 0.012$ is used to integrate Eq. (44) from the beginning time $t = 0$ to the final time $t = 12\,\mathrm{s}$.

The time histories of the vertical displacements measured at the five points Z1, Z3, Z5, Z7, Z9 are depicted in Fig. 4. The mean value of the numerical time histories shows a good agreement with the experimental data [5]. This demonstrates the validity of the mathematical model and numerical scheme developed in this paper. It has been observed that there is a high-frequency oscillation component on the numerical curves (solid lines) and a large initial displacement discrepancy at point Z7. This is due to the different initial conditions of the experiment and the numerical simulation. In the experiment, the carriage was placed on the floating plate model before the experiment started so the floating plate model and the carriage were in their initial static equilibrium state. However, in the numerical simulation, the landing beam with a zero vertical velocity lands on the floating beam at the initial time. The landing beam behaves a suddenly added mass onto the floating beam, which causes an initial dynamic deflection of the floating beam. This dynamic deflection is twice large as

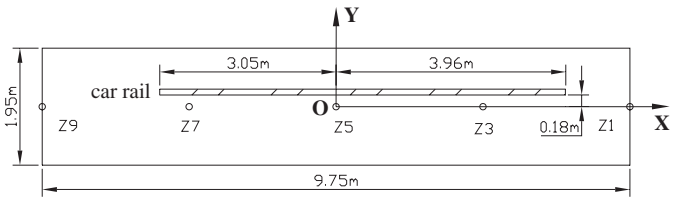

Fig. 3. Arrangements of displacement measure points and car moving rail on the model.

Table 1
Particulars of the floating plate model

Length (L) × breadth (B) × thickness (h)	$9.75 \times 1.95 \times 0.0545\,\mathrm{m}$
Draft (d)	0.0163 m
Bending rigidity ($E_f I_f$)	$17.53\,\mathrm{kN\,m^2}$

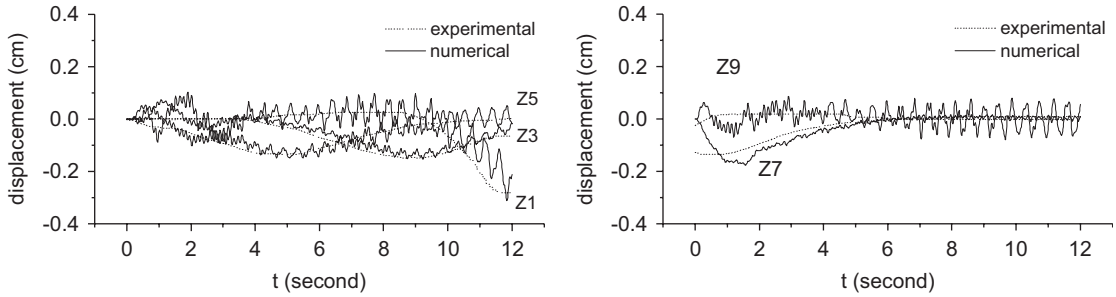

Fig. 4. Time histories of the vertical displacements measured at five points.

the one produced by the static carriage in the test, which produces the oscillation. Due to neglecting the damping of structures and water in the numerical simulation, the oscillation caused by the initial impact does not decrease with the time going.

7.2. An example simulating aircraft landing impacts

In this numerical example, the following geometrical and physical parameters are used.

Landing beam: $E_l I_l = 2 \times 10^2\,\mathrm{Nm}^2$, $m_l = 20\,\mathrm{kg/m}$, $l = 1\,\mathrm{m}$, $V_{Z0} = -0.1\,\mathrm{m/s}$, $V_{X0} = 2\,\mathrm{m/s}$, $a_X = -0.4\,\mathrm{m/s}^2$, $\bar{X}_0 = -2.5\,\mathrm{m}$, $\bar{Z}_0 = 0.15\,\mathrm{m}$, $M_l = 16$.

Floating beam: $E_l I_l = 2 \times 10^3\,\mathrm{Nm}^2$, $m_l = 50\,\mathrm{kg/m}$, $L = 15\,\mathrm{m}$, $h = 0.1\,\mathrm{m}$, $d = 0.05\,\mathrm{m}$, $M_f = 16$.

Support system: $K = 2.0 \times 10^4\,\mathrm{N/m}$, $C = 1.0 \times 10^4\,\mathrm{N\,s/m}$, $l_K = 0.1\,\mathrm{m}$.

Fluid: $\rho = 1 \times 10^3\,\mathrm{kg/m}^3$, $N_f = 1000$, $N_\Sigma = 40$.

Other input data: $g = 9.8\,\mathrm{m/s}^2$, $\Delta t = 0.005\,\mathrm{s}$, $\alpha = 0.25$, $\delta = 0.5$.

To represent the dynamic responses obtained in non-dimensional forms, the reference length d, pressure $p_0 = \rho g d$, resultant force $F_0 = \rho g d l$ and moment $T_0 = F_0 d$ are chosen. The simulation results obtained in association with some physical explanation to confirm its rationality are shown as follows.

(1) Fig. 5 shows the distribution of the non-dimensional dynamic position W/d and water pressure p_d/p_0 along the floating beam at times $t = 1, 2, 3, 4, 5\,\mathrm{s}$. The dynamic position W/d of the floating beam at different time instant always indicates a minimum value around the transient position of the landing beam, which in turn corresponds to a maximum water pressure value. The dynamic position of the floating beam shows a more flat distribution than that of the water pressure, which is significantly influenced by the bending stiffness $E_f I_f$ of the floating beam and seems not sensitive to other parameters. In Fig. 6, the distribution of the water pressure p_d/p_0 along the floating beam at $t = 3\,\mathrm{s}$ with different $E_f I_f$ values is presented. Less wave profiles are observed in the distribution of the water pressure p_d/p_0 with higher $E_f I_f$ value.

(2) Fig. 7 gives the time histories of the non-dimensional dynamic position W/d and water pressure p_d/p_0 at the middle point of the floating beam. It is found that the dynamic position W/d of the middle point of the floating beam increases until to its maximum value at around 0.6 s and then reduces to its minimum value at around 1.46 s while the landing beam passes the middle point. After this, it gradually tends to its static equilibrium position. The increase phenomenon of the dynamic position W/d of the middle point of the floating beam before around 0.6 s is caused by the elastic deformation of the beam. This can be understood as follows. Assume that the floating beam is rigid. The initial landing impact force produces a down translation of its middle point (mass centre) and a rotation of the beam about the middle point. Therefore, the position of the middle point of the assumed rigid beam can only be down. Now, due to the elasticity effect of the floating beam, an elastic deformation of the beam caused by the landing impact force is added into the rigid motion. As a result of this, the position of any point of the beam depends on the summation result of the rigid motion and the elastic deformation of the beam. Fig. 8 shows the distribution of the non-dimensional dynamic position of the floating beam W/d at the selected time step before 1 s. It is observed that the middle point of the floating beam reaches its maximum position at around 0.6 s.

The initial large fluctuation of the water pressure p_d/p_0 at the middle point of the floating beam is a result of the initial impact of the landing beam. After the third second (600 time step), the fluctuation of the water

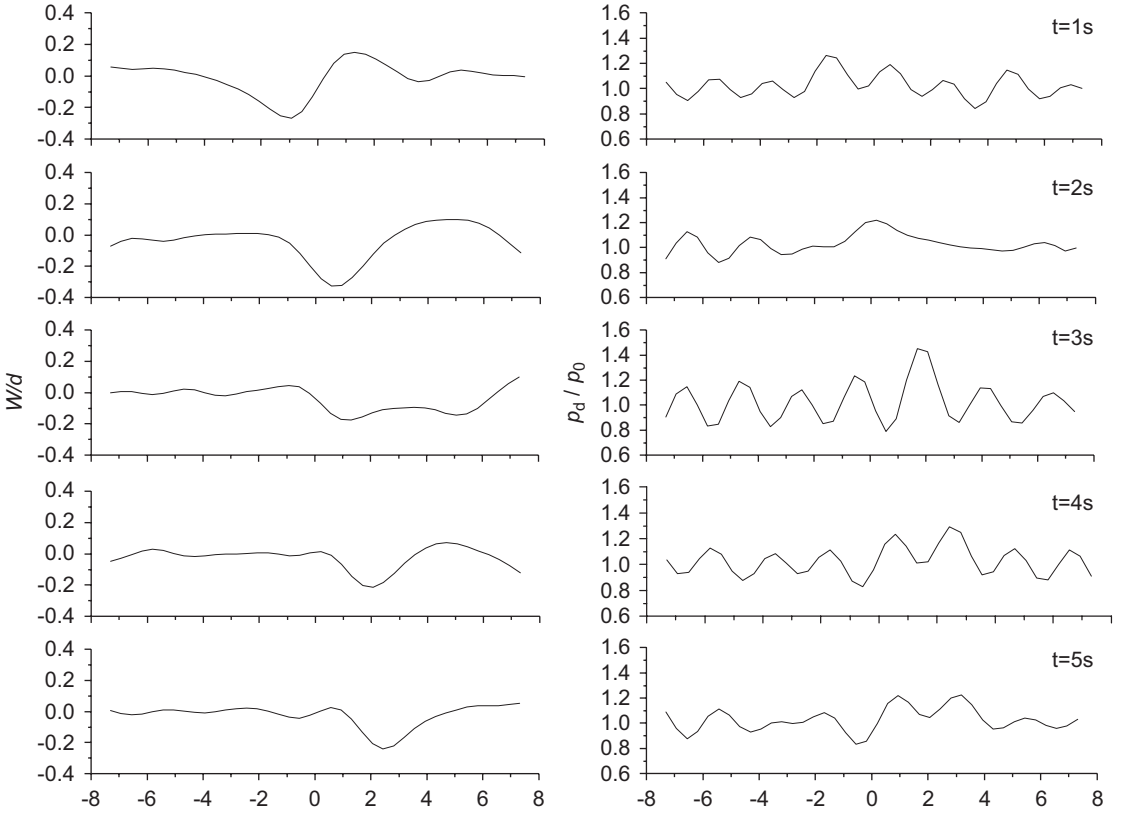

Fig. 5. Distribution of the non-dimensional dynamic position W/d and water pressure p_d/p_0 along the floating beam.

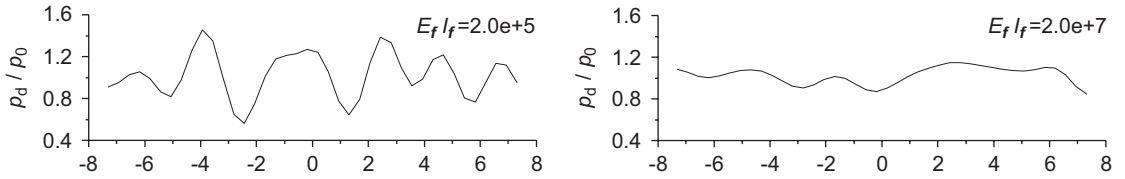

Fig. 6. Distribution of the water pressure p_d/p_0 along the floating beam at $t = 3$ s with different E_fI_f values.

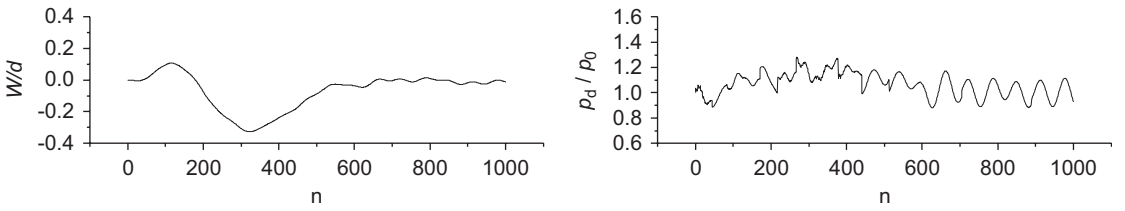

Fig. 7. Time histories of the non-dimensional dynamic position W/d and water pressure p_d/p_0 at the middle point of the floating beam.

pressure becomes relatively stable with an approximate oscillation frequency 2.5 Hz. This frequency is closely related to the motion of the floating beam on the water. With FEA software ANSYS, considering only the hydrostatic force the first-order natural frequency of the floating beam on the water is obtained as 2.19 Hz. The difference between these two frequencies may be due to the fluid–structure coupling effect.

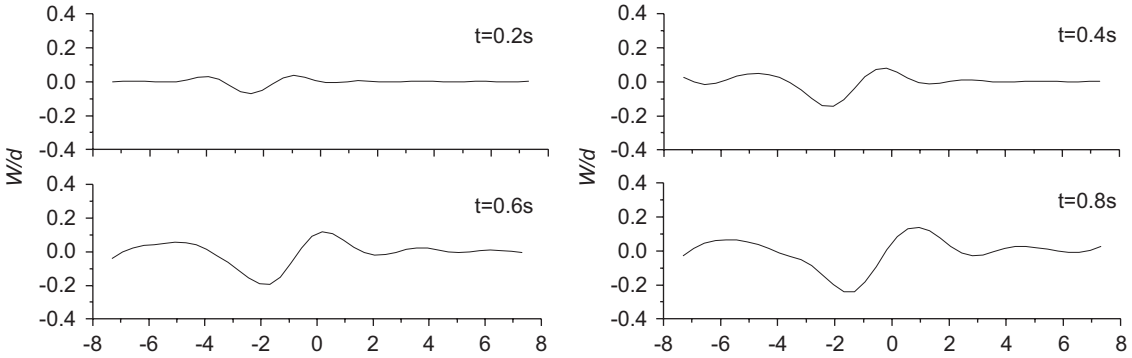

Fig. 8. Distribution of the non-dimensional dynamic position W/d along the floating beam within the first second.

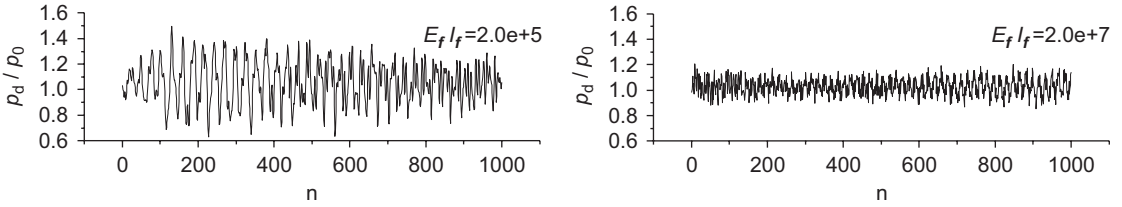

Fig. 9. Time histories of the non-dimensional water pressure p_d/p_0 at the middle point of the floating beam with different bending stiffness E_fI_f of the floating beam.

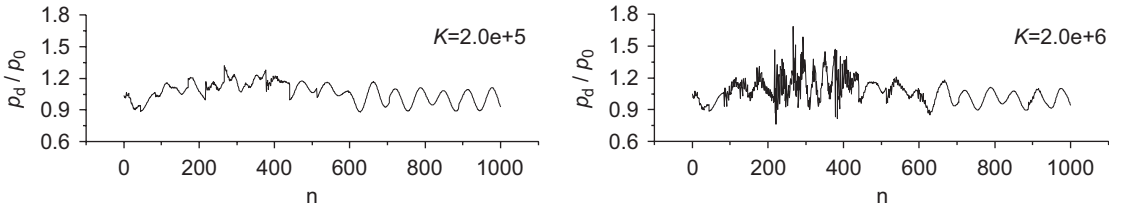

Fig. 10. Time histories of the non-dimensional water pressure p_d/p_0 at the middle point of the floating beam with different spring stiffness K.

Fig. 9 indicates that the oscillation frequency of the water pressure p_d/p_0 at the middle point of the floating beam increases with the increase of the bending stiffness E_fI_f of the floating beam. The effect of spring stiffness K and damping coefficient C of the supporting system on the time history of p_d/p_0 is presented in Figs. 10 and 11, which seems less pronounced than that of the bending stiffness E_fI_f. With the increase of K or C, a high-frequency component seems to be added to the time history of p_d/p_0 especially around the time instant (at 292 time step) when the landing beam passing the middle point of the floating beam. This effect becomes much less significant after the landing beam passes by.

(3) Fig. 12 indicates the time histories of the non-dimensional resultant force of water pressure F_d/F_0 and its moment T_d/T_0 about the middle point of floating beam. It is found the resultant force F_d/F_0 shows a damping oscillation with a relatively stable frequency 7 Hz over the 5 s period. This frequency is larger than the first-order natural frequency 4.31 Hz of the landing system fixed at the end of the supporting system. If the parameters of the landing system are changed, the stable frequency of the resultant force F_d/F_0 has been found a corresponding change. This demonstrates that the stable frequency of the resultant force F_d/F_0 is strongly related to the landing system. Some examples are shown in Figs. 13–16. The moment T_d/T_0 has the same frequency as the resultant force F_d/F_0 and it always resists the moment produced by the landing and translation of the landing beam.

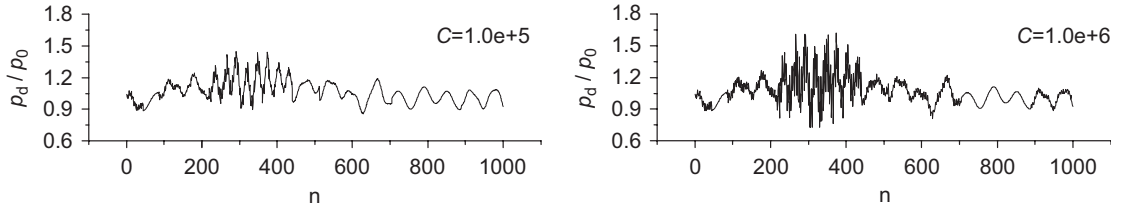

Fig. 11. Time histories of the non-dimensional water pressure p_d/p_0 at the middle point of the floating beam with different damping coefficient C.

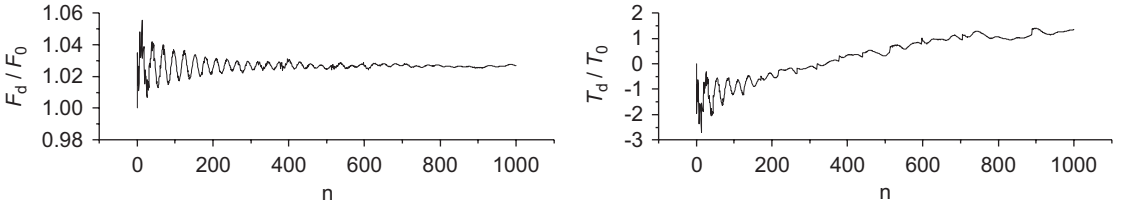

Fig. 12. Time histories of the non-dimensional resultant force F_d/F_0 and its moment T_d/T_0 about the middle point of the floating beam.

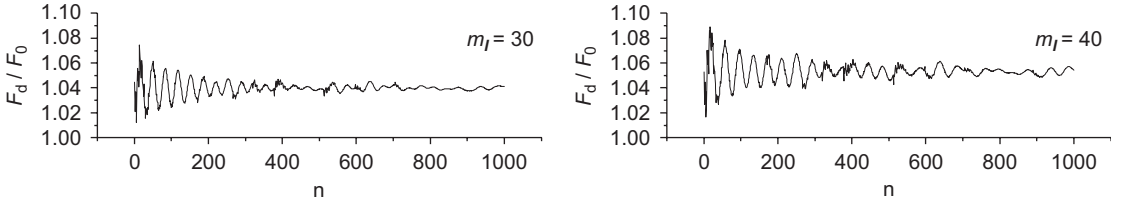

Fig. 13. Time history of the non-dimensional resultant force F_d/F_0 with different mass per unit length m_l of the landing beam.

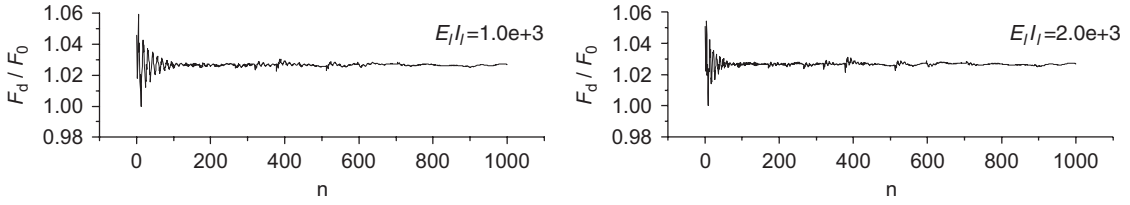

Fig. 14. Time history of the non-dimensional resultant force F_d/F_0 with different bending stiffness E_fI_f of the landing beam.

Figs. 13–16 show the time history of the resultant force F_d/F_0 with different m_l, E_lI_l, K, C of the landing beam, respectively. The frequency of the resultant force F_d/F_0 decreases with the increase of mass per unit length m_l and increases with the increase of the bending stiffness E_lI_l. This frequency shows no change for different spring stiffness K or damping coefficient C. However, a high frequency component is observed with increasing K or C.

(4) Fig. 17 presents the distribution of the non-dimensional dynamic position Z/d of the landing beam at times $t = 1, 2, 3, 4, 5$ s. Figs. 18 and 19 give time histories of the non-dimensional dynamic position Z/d at the middle point of the landing beam and the non-dimensional dynamic force F_i/F_0 provided by the supporting system. The landing beam shows a relatively stable configuration, which is dominated by its gravity. The dynamic position Z/d of the middle point of the landing beam decreases to the minimum value at around

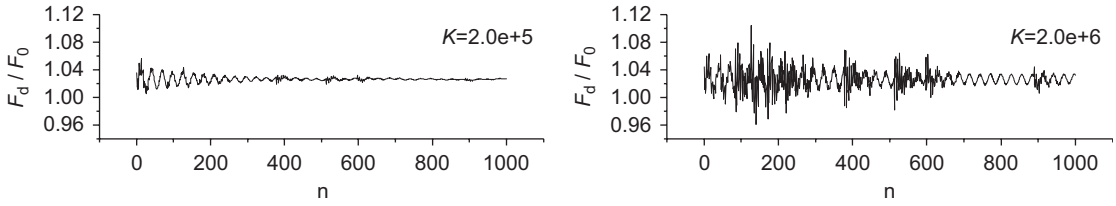

Fig. 15. Time history of the non-dimensional resultant force F_d/F_0 with different spring stiffness K.

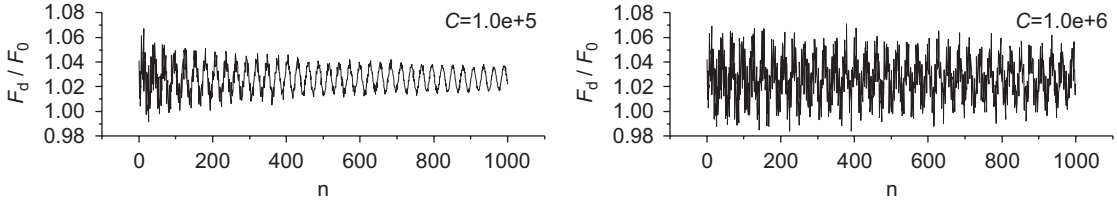

Fig. 16. Time history of the non-dimensional resultant force F_d/F_0 with different damping coefficient C.

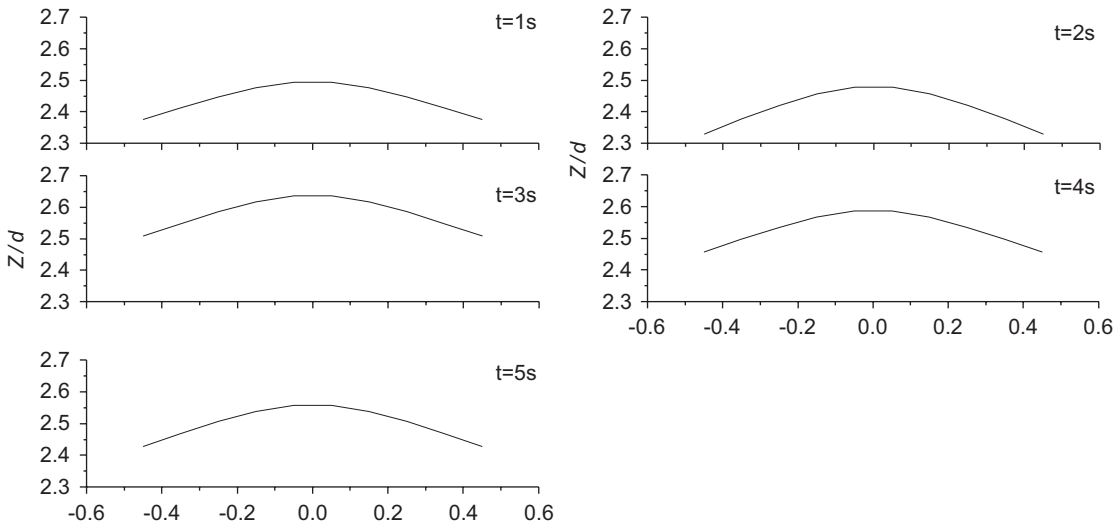

Fig. 17. Distribution of the non-dimensional dynamic position Z/d along the landing beam.

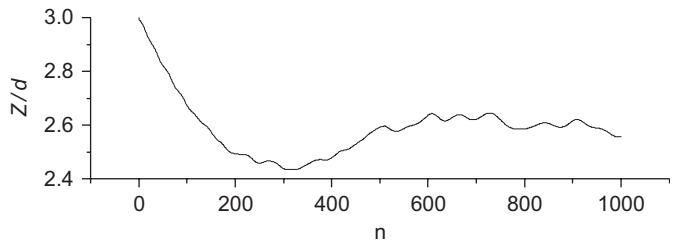

Fig. 18. Time history of the non-dimensional dynamic position Z/d at the middle point of the landing beam.

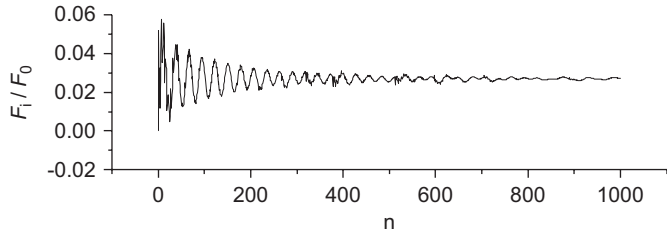

Fig. 19. Time history of the non-dimensional dynamic force F_i/F_0 provided by the supporting system.

$t = 1.5$ s and then increases to its equilibrium value. The dynamic force F_i/F_0 provided by the supporting system indicates a damping oscillation with the same frequency but different amplitude of the resultant force F_d/F_0.

8. Conclusions

A mixed mode function-boundary element method has been proposed to numerically solve the dynamic responses of a landing beam–floating beam–water interaction system excited by the landing beam. The two beams are considered as two solid substructures of which the motions are represented by their mode functions and the water domain is modelled by a boundary element method. The coupled fluid–structure motion equation is solved with the Newmark assumptions.

The responses of this landing beam–floating beam–water interaction system are obtained from the numerical calculations. The dynamic position and the hydrodynamic pressure distribution along the floating beam at different time instant clearly indicate the travelling effect of the landing beam; the large initial values of the hydrodynamic pressure, the resultant hydrodynamic force and its moment illustrate the effect of the landing impact. The distribution of the hydrodynamic pressure along the floating beam at each time instant is sensitive to the bending stiffness of the floating beam; the stable frequency of the hydrodynamic pressure at the middle point of the floating beam is related to the motion of the floating beam on the water; the frequency of the resultant hydrodynamic force is related to the landing system.

The numerical results illustrate the rationality and feasibility of the mathematical model and numerical formulations derived in this paper. The proposed mixed mode function-boundary element method is proved to be a practical technique to solve a real aircraft–floating structure–water interaction system excited by aircraft landing impacts.

Acknowledgement

Authors gratefully acknowledge Prof. W.G. Price for his modification and suggestion in preparing the manuscript of the paper.

Appendix A

As observed in Eqs. (38) and (44), the fluid–structure interaction equations are coupled through the first order time derivatives $\ddot{\boldsymbol{\Psi}}_2$ and $\dot{\mathbf{Q}}$. To solve these coupled equations, we intend to express $\ddot{\boldsymbol{\Psi}}_2$ as a function of $\dot{\mathbf{Q}}$ and other obtained values at the previous time step. The Newmark's formulation [15] provides a bridge to realise our aim. Using Newmark's formulation, the velocity potential $\boldsymbol{\Psi}^{(t)}$ and its first-order derivative $\dot{\boldsymbol{\Psi}}^{(t)}$ with respect to time are expressed as

$$\dot{\boldsymbol{\Psi}}^{(t)} = \dot{\boldsymbol{\Psi}}^{(t-\Delta t)} + [(1-\delta)\ddot{\boldsymbol{\Psi}}^{(t-\Delta t)} + \delta\ddot{\boldsymbol{\Psi}}^{(t)}]\Delta t, \tag{A.1}$$

$$\boldsymbol{\Psi}^{(t)} = \boldsymbol{\Psi}^{(t-\Delta t)} + \dot{\boldsymbol{\Psi}}^{(t-\Delta t)}\Delta t + \left[\left(\tfrac{1}{2}-\alpha\right)\ddot{\boldsymbol{\Psi}}^{(t-\Delta t)} + \alpha\ddot{\boldsymbol{\Psi}}^{(t)}\right]\Delta t^2, \tag{A.2}$$

where α and δ are two Newmark parameters and Δt denotes time step. From these two formulations (A.1) and (A.2), $\boldsymbol{\Psi}^{(t)}$ and $\ddot{\boldsymbol{\Psi}}^{(t)}$ are obtained as

$$\boldsymbol{\Psi}^{(t)} = a_1\dot{\boldsymbol{\Psi}}^{(t)} + \boldsymbol{\Psi}^{(t-\Delta t)} + a_2\dot{\boldsymbol{\Psi}}^{(t-\Delta t)} + a_3\ddot{\boldsymbol{\Psi}}^{(t-\Delta t)}, \tag{A.3}$$

$$\ddot{\boldsymbol{\Psi}}^{(t)} = a_4[\dot{\boldsymbol{\Psi}}^{(t)} - \dot{\boldsymbol{\Psi}}^{(t-\Delta t)}] + a_5\ddot{\boldsymbol{\Psi}}^{(t-\Delta t)}, \tag{A.4}$$

where $a_1 = \alpha\Delta t/\delta$, $a_2 = (1-\alpha/\delta)\Delta t$, $a_3 = (1/2-\alpha/\delta)\Delta t^2$, $a_4 = 1/\delta\Delta t$, $a_5 = 1-1/\delta$.

The substitution of Eqs. (A.3) and (A.4) into Eq. (38) yields an equation

$$\dot{\boldsymbol{\Psi}}^{(t)} = \mathbf{C}\dot{\mathbf{Q}}(t) + \mathbf{A}\boldsymbol{\Psi}^{(t-\Delta t)} + \mathbf{B}\dot{\boldsymbol{\Psi}}^{(t-\Delta t)} + \mathbf{D}\ddot{\boldsymbol{\Psi}}^{(t-\Delta t)}, \tag{A.5}$$

where the coefficient matrices are defined as

$$\begin{aligned} &\mathbf{A} = -\mathbf{E}\mathbf{H}, \quad \mathbf{B} = \mathbf{E}[a_4\mathbf{G} - a_2\mathbf{H}], \quad \mathbf{C} = \mathbf{E}\tilde{\mathbf{G}}, \\ &\mathbf{D} = -\mathbf{E}[a_5\mathbf{G} + a_3\mathbf{H}], \quad \mathbf{E} = [a_4\mathbf{G} + a_1\mathbf{H}]^{-1}. \end{aligned} \tag{A.6}$$

Following the definition in Eq. (41), Eq. (A.5) is rewritten as

$$\begin{bmatrix} \dot{\boldsymbol{\Psi}}_1^{(t)} \\ \dot{\boldsymbol{\Psi}}_2^{(t)} \\ \dot{\boldsymbol{\Psi}}_3^{(t)} \end{bmatrix} = \begin{bmatrix} \mathbf{C}_1 \\ \mathbf{C}_2 \\ \mathbf{C}_3 \end{bmatrix} \dot{\mathbf{Q}}(t) + \begin{bmatrix} \mathbf{A}_1 \\ \mathbf{A}_2 \\ \mathbf{A}_3 \end{bmatrix} \boldsymbol{\Psi}^{(t-\Delta t)} + \begin{bmatrix} \mathbf{B}_1 \\ \mathbf{B}_2 \\ \mathbf{B}_3 \end{bmatrix} \dot{\boldsymbol{\Psi}}^{(t-\Delta t)} + \begin{bmatrix} \mathbf{D}_1 \\ \mathbf{D}_2 \\ \mathbf{D}_3 \end{bmatrix} \ddot{\boldsymbol{\Psi}}^{(t-\Delta t)} \tag{A.7}$$

from which it follows that

$$\dot{\boldsymbol{\Psi}}_2^{(t)} = \mathbf{C}_2\dot{\mathbf{Q}}(t) + \mathbf{A}_2\boldsymbol{\Psi}^{(t-\Delta t)} + \mathbf{B}_2\dot{\boldsymbol{\Psi}}^{(t-\Delta t)} + \mathbf{D}_2\ddot{\boldsymbol{\Psi}}^{(t-\Delta t)}. \tag{A.8}$$

The substitution of Eq. (A.8) into Eq. (44) produces

$$\begin{aligned} &\begin{bmatrix} M^{(t)} & \mathbf{0} \\ \mathbf{0} & \mathbf{M}^{(f)} \end{bmatrix} \begin{bmatrix} \ddot{\mathbf{q}}(t) \\ \ddot{\mathbf{Q}}(t) \end{bmatrix} + \begin{bmatrix} \mathbf{C}^{(ll)} & \mathbf{C}^{(lf)}(t) \\ \mathbf{C}^{(fl)}(t) & \mathbf{C}^{(ff)}(t) + \mathbf{C}^d\mathbf{C}_2 \end{bmatrix} \begin{bmatrix} \dot{\mathbf{q}}(t) \\ \dot{\mathbf{Q}}(t) \end{bmatrix} \\ &\quad + \begin{bmatrix} \mathbf{K}^{(l)} + \mathbf{K}^{(ll)} & \mathbf{K}^{(lf)}(t) \\ \mathbf{K}^{(fl)}(t) & \mathbf{K}^{(f)} + \mathbf{K}^{(ff)}(t) + \mathbf{K}^d \end{bmatrix} \begin{bmatrix} \mathbf{q}(t) \\ \mathbf{Q}(t) \end{bmatrix} \\ &= \begin{bmatrix} \mathbf{F}_g^{(l)} \\ -\mathbf{C}^d\left(\mathbf{A}_2\boldsymbol{\Psi}^{(t-\Delta t)} + \mathbf{B}_2\dot{\boldsymbol{\Psi}}^{(t-\Delta t)} + \mathbf{D}_2\ddot{\boldsymbol{\Psi}}^{(t-\Delta t)}\right) \end{bmatrix}. \end{aligned} \tag{A.9}$$

In this equation, there is a non-symmetrical term $\mathbf{C}^d\mathbf{C}_2$ caused by fluid–structure interaction. Therefore, the traditional Newark solution procedure based on symmetrical matrices is not applicable. As an approximation in engineering analysis, the non-symmetrical term $\mathbf{C}^d\mathbf{C}_2\dot{\mathbf{Q}}(t)$ may be moved to the right hand side of Eq. (A.9) and its values at time t is approximately replaced by the value at the previous time step $t-\Delta t$. This approximation avoids solving a large non-symmetrical matrix equation but not losing necessary accuracy accepted in engineering [16]. However, for the simple example investigated in this paper, the non-symmetrical Eq. (A.9) is directly solved without the discussed approximate treatment. For this end, using Newmark's formulation again, we express the generalised acceleration $\ddot{\mathbf{q}}(t)$, $\ddot{\mathbf{Q}}(t)$ and velocity $\dot{\mathbf{q}}(t)$, $\dot{\mathbf{Q}}(t)$ in the forms

$$\begin{bmatrix} \ddot{\mathbf{q}}(t) \\ \ddot{\mathbf{Q}}(t) \end{bmatrix} = a_6\left(\begin{bmatrix} \mathbf{q}(t) \\ \mathbf{Q}(t) \end{bmatrix} - \begin{bmatrix} \mathbf{q}(t-\Delta t) \\ \mathbf{Q}(t-\Delta t) \end{bmatrix}\right) - a_7\begin{bmatrix} \dot{\mathbf{q}}(t-\Delta t) \\ \dot{\mathbf{Q}}(t-\Delta t) \end{bmatrix} - a_8\begin{bmatrix} \ddot{\mathbf{q}}(t-\Delta t) \\ \ddot{\mathbf{Q}}(t-\Delta t) \end{bmatrix}, \tag{A.10}$$

$$\begin{bmatrix} \dot{\mathbf{q}}(t) \\ \dot{\mathbf{Q}}(t) \end{bmatrix} = a_9\left(\begin{bmatrix} \mathbf{q}(t) \\ \mathbf{Q}(t) \end{bmatrix} - \begin{bmatrix} \mathbf{q}(t-\Delta t) \\ \mathbf{Q}(t-\Delta t) \end{bmatrix}\right) - a_{10}\begin{bmatrix} \dot{\mathbf{q}}(t-\Delta t) \\ \dot{\mathbf{Q}}(t-\Delta t) \end{bmatrix} - a_{11}\begin{bmatrix} \ddot{\mathbf{q}}(t-\Delta t) \\ \ddot{\mathbf{Q}}(t-\Delta t) \end{bmatrix}, \tag{A.11}$$

where $a_6 = 1/\alpha\Delta t^2$, $a_7 = 1/\alpha\Delta t$, $a_8 = (1/2\alpha) - 1$, $a_9 = \delta/\alpha\Delta t$, $a_{10} = (\delta/\alpha) - 1$ and $a_{11} = \Delta t/2((\delta/\alpha) - 2)$.

Substituting Eqs. (A.10) and (A.11) into Eq. (A.9), we obtain a time integration equation:

$$\left[\tilde{\mathbf{K}} + a_6\tilde{\mathbf{M}} + a_9\tilde{\mathbf{C}}\right]\begin{bmatrix}\mathbf{q}(t)\\ \mathbf{Q}(t)\end{bmatrix} = \mathbf{R}^{(t-\Delta t)} + \mathbf{R}_{\mathbf{a}}^{(t-\Delta t)} + \mathbf{R}_{\mathbf{v}}^{(t-\Delta t)}, \tag{A.12}$$

where

$$\tilde{\mathbf{K}} = \begin{bmatrix}\mathbf{K}^{(l)} + \mathbf{K}^{(ll)} & \mathbf{K}^{(lf)}(t)\\ \mathbf{K}^{(fl)}(t) & \mathbf{K}^{(f)} + \mathbf{K}^{(ff)}(t) + \mathbf{K}^{d}\end{bmatrix}, \tag{A.13}$$

$$\tilde{\mathbf{M}} = \begin{bmatrix}\mathbf{M}^{(l)} & \mathbf{0}\\ \mathbf{0} & \mathbf{M}^{(f)}\end{bmatrix}, \tag{A.14}$$

$$\tilde{\mathbf{C}} = \begin{bmatrix}\mathbf{C}^{(ll)} & \mathbf{C}^{(lf)}(t)\\ \mathbf{C}^{(fl)}(t) & \mathbf{C}^{(ff)}(t) + \mathbf{C}^{d}\mathbf{C}_2\end{bmatrix}, \tag{A.15}$$

$$\mathbf{R}^{(t-\Delta t)} = \begin{bmatrix}\mathbf{F}_g^{(l)}\\ -\mathbf{C}^{d}\left(\mathbf{A}_2\boldsymbol{\Psi}^{(t-\Delta t)} + \mathbf{B}_2\dot{\boldsymbol{\Psi}}^{(t-\Delta t)} + \mathbf{D}_2\ddot{\boldsymbol{\Psi}}^{(t-\Delta t)}\right)\end{bmatrix}, \tag{A.16}$$

$$\mathbf{R}_{\mathbf{a}}^{(t-\Delta t)} = \tilde{\mathbf{M}}\left\{a_6\begin{bmatrix}\mathbf{q}\\ \mathbf{Q}\end{bmatrix}^{(t-\Delta t)} + a_7\begin{bmatrix}\dot{\mathbf{q}}\\ \dot{\mathbf{Q}}\end{bmatrix}^{(t-\Delta t)} + a_8\begin{bmatrix}\ddot{\mathbf{q}}\\ \ddot{\mathbf{Q}}\end{bmatrix}^{(t-\Delta t)}\right\}, \tag{A.17}$$

$$\mathbf{R}_{\mathbf{v}}^{(t-\Delta t)} = \tilde{\mathbf{C}}\left\{a_9\begin{bmatrix}\mathbf{q}\\ \mathbf{Q}\end{bmatrix}^{(t-\Delta t)} + a_{10}\begin{bmatrix}\dot{\mathbf{q}}\\ \dot{\mathbf{Q}}\end{bmatrix}^{(t-\Delta t)} + a_{11}\begin{bmatrix}\ddot{\mathbf{q}}\\ \ddot{\mathbf{Q}}\end{bmatrix}^{(t-\Delta t)}\right\}. \tag{A.18}$$

Eqs. (A.5), (A.8) and (A.12) construct a set of time integration equations to solve the mixed mode function-boundary element equations describing this complex transient dynamic system.

References

[1] E. Watanabe, T. Utsunomiya, Transient response analysis of a VLFS at airplane landing, *Proceedings of the Second International Workshop On Very Large Floating Structures*, Hayama, Japan, 1996, pp. 243–247.

[2] J.W. Kim, W.C. Webster, The drag of an airplane taking off from a floating runway, *Proceedings of the Second International Workshop On Very Large Floating Structures*, Hayama, Japan, 1996, pp. 235–241.

[3] R.W. Yeung, J.W. Kim, Structural drag and deformation of a moving load on a floating plate, *Proceedings of the Second Hydroelasticity in Marine Technology*, Fukuoka, Japan, 1998, pp. 77–88.

[4] S. Ohmatsu, Numerical calculation of hydroelastic behaviour of VLFS in time domain, *Proceedings of the Second Hydroelasticity in Marine Technology*, Fukuoka, Japan, 1998, pp. 89–97.

[5] H. Endo, K. Yago, Time history response of a large floating structure subjected to dynamic load, *Journal of the Society of Naval Architects of Japan* 186 (1998) 369–376.

[6] M. Kashiwagi, Transient responses of a VLFS during landing and take-off of an airplane, *Journal of Marine Science and Technology* 9 (2004) 14–23.

[7] M. Kashiwagi, A time-domain mode-expansion method for calculating transient elastic responses of a pontoon-type VLFS, *Journal of Marine Science and Technology* 5 (2000) 89–100.

[8] J.T. Xing, J.Z. Jin, A mixed mode function-boundary element method for the transient impact analysis of an aircraft landing on a floating structure, *Proceedings of the Ninth International Symposium on Practical Design of Ships and Other Floating Structures*, Luebeck-Travemuende, Germany, 2004, pp. 819–826.

[9] J.T. Xing, J. Jin, A dynamic analysis of an integrated aircraft–floating structure–water interaction system excited by the impact of an aircraft landing, *Proceedings of the 15th International Offshore and Polar Engineering Conference,* Vol. 1, Seoul, Korea, 2005, pp. 182–189.

[10] J.N. Newman, Wave effects on deformable bodies, *Journal of Applied Ocean Research* 16 (1994) 47–59.

[11] J.T. Xing, W.G. Price, M.J. Pomfret, L.H. Yam, Natural vibration of a beam–water interaction system, *Journal of Sound and Vibration* 199 (3) (1997) 491–512.
[12] A. Sommerfeld, *Partial Differential Equations in Physics*, Academic Press INC. Publishers, New York, 1949.
[13] C.A. Brebbia, *The Boundary Element Method for Engineers*, Pentech Press, London, 1980.
[14] W. Kaplan, *Advanced Calculus*, Addison-Wesley, Cambridge, MA, 1984.
[15] N.M. Newmark, A method of computation for structural dynamics, *Journal of Engineering Mechanics Division—ASCE* 85 (1959) 67–94.
[16] K.-J. Bathe, *Finite Element Procedures*, Prentice-Hall, Englewood Cliffs, NJ, 1996.